Waveform inversion combining one-way and two-way wave-equation migration

Xin Fu, Sergio Romahn, Kris Innanen

ABSTRACT

Full waveform inversion (FWI), which considers dynamic and kinematic information of seismic wave simultaneously, helps to interpret detailed characteristics of the subsurface. Growing out from FWI, iterative modelling, migration, and inversion (IMMI) considers waveform inversion as a cyclical process of the migration and standard inversion. In IMMI, any type of depth migration is available, which gives greater convenience to waveform inversion. Much research has shown that IMMI with the control of well log data is an effective method for waveform inversion. However, how to perform IMMI in the absence of well log data has not systematically investigated. In this paper, we examine IMMI in the absence of well log data. we introduce how to choose impedance inversion algorithms in IMMI for different depth migration algorithms. And we suggest employing the trace integration algorithm in frequency domain for a one-way depth migration based on the one-way wave equation, and the impedance inversion algorithm without phase change for a two-way depth migration based on the two-way wave equation. In our research, the one-way depth migration algorithm used is phase shift plus interpolation (PSPI) migration, and the two-way depth migration algorithm used is reverse time migration (RTM). Built on this, we develop a combined IMMI method which uses the one-way depth migration and the two-way depth migration sequentially in IMMI. To do comparisons between FWI, IMMI using PSPI migration, IMMI using RTM, and the combined IMMI method, two numerical examples are used. The comparisons show that IMMI using RTM and using PSPI are better than FWI, and the best wave to implement waveform inversion in the absence of well log data is the combined IMMI method.

INTRODUCTION

With the increasing of exploration requirements, more powerful seismic inversion tool is needed. As a potential power to recover physical properties of subsurface rock, full waveform inversion (FWI), introduced to seismic exploration by Lailly and Bednar (1983) and Tarantola (1984), is researched widely and developing fast (Virieux and Operto, 2009). Since FWI considers dynamic and kinematic information of seismic wave simultaneously, it helps to interpret very detailed characteristics of the subsurface. In the frame of FWI, one of the key steps is producing the gradient from forward and backward wavefields, which is similar with reverse time migration (RTM). Based on this frame, Margrave et al. (2010, 2011b) propose to use any depth migration algorithm to obtain the gradient, and phase shift plus interpolation (PSPI) migration based the one-way wave equation is used in his example. Furthermore, in 2012, he summarized iterative modelling, migration, and inversion (IMMI) as a viable step forward of FWI, in which both well validation and data validation can be utilized and any migration algorithm is allowed (Margrave et al., 2012). Behind him, Pan et al. (2014), Margrave et al. (2011b), Guarido et al. (2015), Arenrin and Margrave (2015), and Romahn and Innanen (2017, 2018) have developed IMMI method and pretty good effects are achieved. However, all the works mentioned above belongs

to well validation which applies well log data as a calibration of the gradient from depth migration. Although Romahn and Innanen (2018) test the data validation method using only PSPI migration without the control of well log, the result is not satisfactory.

In this paper, we examine the IMMI method in the absence of well log data. First, we review the FWI and IMMI method, then we discuss how to choose impedance inversion algorithms in IMMI for different depth migration algorithms. We also develop a combined IMMI method: using the one-way depth migration (PSPI) and the two-way depth migration (RTM) sequentially in IMMI. Finally, we use two numerical examples to do comparisons between FWI, IMMI using PSPI, IMMI using RTM and the combined IMMI method.

Full waveform inversion (FWI)

Full waveform inversion (FWI) as an iterative inversion mothed estimates subsurface parameters by matching synthetic data ($\mathbf{u}_{syn}(\mathbf{m})$) , a function of model parameter $\mathbf{m}$, with observed data. The most common way to accomplish this is minimizing the L2 norm of data residual $\delta\mathbf{u}$ ($\mathbf{u}_{syn}(\mathbf{m}) - \mathbf{u}_{obs}$):

$$E(\mathbf{m}) = \frac{1}{2}\delta\mathbf{u}^T\delta\mathbf{u}. \tag{1}$$

The misfit function $E(\mathbf{m})$ depends on the model parameter $\mathbf{m}$. Within the framework of Born approximation, the updated model $\mathbf{m}$ is seen as a sum of reference model $\mathbf{m}_0$ and model perturbation $\Delta\mathbf{m}$ during the iterative inversion process. Using Taylor expansion and ignoring things behind and including second-order term, we obtain linearized formula:

$$E(\mathbf{m}) = E(\mathbf{m}_0) + \frac{\partial E(\mathbf{m}_0)}{\partial \mathbf{m}}\Delta\mathbf{m}. \tag{2}$$

Continuously, taking the derivative with respect to $\mathbf{m}$, we have:

$$\frac{\partial E(\mathbf{m})}{\partial \mathbf{m}} = \frac{\partial E(\mathbf{m}_0)}{\partial \mathbf{m}} + \frac{\partial^2 E(\mathbf{m}_0)}{\partial \mathbf{m}^2}\Delta\mathbf{m}. \tag{3}$$

Setting the derivative as zero to minimize the above objective function, and after easy algebraic operations, we obtain:

$$\Delta\mathbf{m} = -\mathbf{H}^{-1}\mathbf{g}, \tag{4}$$

where $\mathbf{H} = \dfrac{\partial^2 E(\mathbf{m}_0)}{\partial \mathbf{m}^2}$ and $\mathbf{g} = \dfrac{\partial E(\mathbf{m}_0)}{\partial \mathbf{m}}$ are Hessian matrix and Jacobian matrix, respectively. To avoid the expensive computation of inversion Hessian matrix, gradient-based methods use identical matrix $\mathbf{I}$ as an approximate substitution of $\mathbf{H}$, such as steepest-descent (SD) method and non-linear conjugate gradient (NCG) method (Mora, 1987; Tarantola, 1984; Crase et al., 1990; Hu et al., 2011). In this paper, we apply the SD method for FWI, which helps to converge globally (Hu et al., 2011), and the corresponding model perturbation with step length can be expressed as:

$$\Delta\mathbf{m} = -\mu\mathbf{g}. \tag{5}$$

It is the negative direction of gradient and the step length μ is a constant calculated via line-search method. Here we use parabolic fit to obtain the step length, which can save

computing cost (Vigh et al., 2009; Romahn and Innanen, 2018). Also, we precondition the gradient with deconvolution imaging condition to compensate the spherical spreading of seismic wave (Margrave et al., 2011a), which can achieve the similar effect to that of approximate inverse Hessian of Shin et al. (2001) but avoid the calculation of Hessian.

Furthermore, for an acoustic waveform inversion with constant density in this paper, when the model $\mathbf{m}$ represents slowness of the subsurface medium, the specified expression for the gradient $\mathbf{g}$ expressed as a function of location $g(\mathbf{x})$ in time domain is (Tarantola, 1984; Yang et al., 2015):

$$g(\mathbf{x}) = \sum_{r=1}^{ng} \sum_{i=1}^{ns} \int_0^{t_{max}} dt \left[-2s(\mathbf{x}) \frac{\partial^2 u_{syn}(\mathbf{x}, t; \mathbf{x}_s)}{\partial t^2} \delta u(\mathbf{x}, t; \mathbf{x}_r) \right]. \tag{6}$$

where ng, ns is the number of receivers and shots, respectively; t_{max} is the maximum forward/back ward propagating time t of wavefield; $\mathbf{x}$, $\mathbf{x_s}$, $\mathbf{x_r}$ is the location matrix in the model place as a whole, the location matrix for sources, and the location matrix for receivers, respectively; and s is the model slowness as a function of location $\mathbf{x}$; $u_{syn}(\mathbf{x}, t; \mathbf{x}_s)$ is forward wavefield with the source wavelet used to active the shots at location $\mathbf{x}_s$, and $\delta u(\mathbf{x}, t; \mathbf{x}_r)$ is backward/time-reversal wavefield using the data residual at location $\mathbf{x}_r$ as the source.

Iterative modeling migration and inversion (IMMI)

Iterative Modelling Migration and Inversion (IMMI) evolved from FWI establishes the connection between seismic processing and interpretation. This method is developed by Margrave et al. (2012), which is a cooperation process between depth migration and standard methodology (SM), and he describes the algorithm of IMMI as six steps below:

1. Prepare the data. If the modelling to be done uses limited physics, for example acoustic modelling for land data, then this dictates at least some of the processing. Ground roll may need to be suppressed and deconvolution may be required. Strongly nonstationary data may benefit from an inverse Q filter or a Gabor deconvolution. An effort should be made to estimate the wavelet at the end of this step.

2. Build initial background model as a very smooth migration model. The background model should be capable to replicating the data first breaks but should show almost no reflections. This model becomes the current model for the first iteration.

3. Create synthetic seismic data with the current model and the geometry of the real seismic data using the current wavelet estimate. Generally, this will be done with finite difference modelling.

4. Migrate the data difference with a prestack depth migration. Initially migrate only the lowest frequencies. As the iteration proceeds move up the frequency band. We recommend using an f-x migration algorithm like phase shift plus interpolation (PSPI) migration Gazdag and Sguazzero (1984) with a deconvolution imaging condition. Stack the migrated shot records with whatever mute seem appropriate.

5. Convert the migrated stack into a velocity update either through a line search or, if well control is available, by tying the stack to logs. A mixture of both methods may prove useful. If tying to wells, then a wavelet update may also be obtained. The procedure using well control is essentially analogous to standard impedance inversion.

6. Update both velocity model and wavelet and repeat steps 3-6 as often as desired.

The core thought of IMMI is applying a better velocity model to redo the migration where the reflectivity residual comes from. IMMI utilizes the depth migration with deconvolution image condition to data residual to generate a crude version of reflectivity residual, then use the impedance inversion algorithm to convert the reflectivity residual to impedance perturbation or velocity perturbation if density is constant, then cycle this process. One exciting thing is that any depth migration is allowed in this algorithm.

In this paper, we use IMMI for the case of isotropic medium based on the constant-density acoustic equation, utilize modeling data of the true model instead of real field seismic data, and the wavelet is known as well, so we do not need any processing in step 1. In step 4, the one-way wave-equation based f-x migration algorithm and multiscale inversion strategy are recommended. The f-x migration provides great convenience for multiscale strategy to select a specific frequency range. In our study, we use both PSPI migration based on the one-way wave equation and reverse time migration (RTM) based on the one-way wave equation in step 4. Step 5 is the impedance inversion, if well log data is available, then it can be used to calibrate the impedance/velocity perturbation, including obtaining the step length and fixing phase misfit problem caused by the one-way migration, such as the phase shift in PSPI migration (Pan et al., 2014; Romahn and Innanen, 2018). Hereon, to employ IMMI in the absence of well log data, we use only line search to obtain the step length, which is the same as FWI introduced above. Different from the case of well control in which the impedance inversion algorithm is unconstrained, the selection of inversion algorithm in the absence of well control depends both on the properties of migration method and impedance inversion algorithm. This is discussed in detail below.

Choosing impedance inversion algorithms for different migration algorithms

The result of depth migration with deconvolution image condition is regarded as a crude version of reflection coefficients whose relation between impedance is:

$$R_i = \frac{I_{i+1} - I_i}{I_{i+1} + I_i} \tag{7}$$

This is a 1D equation where R_i is the reflectivity for i^{th} interface, and I_i, I_{i+1} is the impedance of i^{th} and $(i+1)^{th}$ layer, respectively. In this paper, the parameterization is slowness s , so the corresponding reflectivity equation is:

$$R_i = -\frac{s_{i+1} - s_i}{s_{i+1} + s_i} = -\frac{\Delta s}{2s}, \tag{8}$$

or

$$\Delta \ln s \approx -2R_i, \tag{9}$$

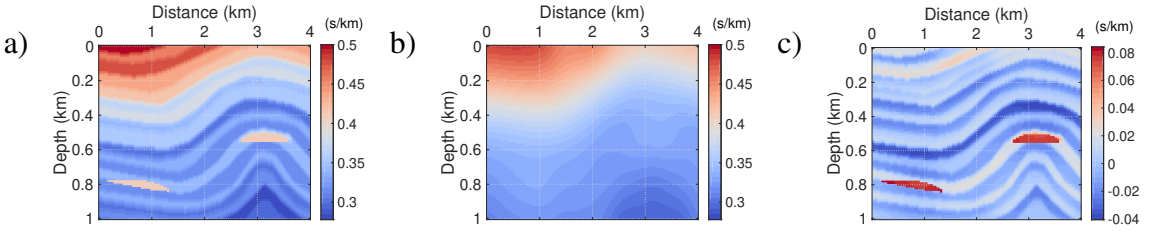

FIG. 1. (a) The true slowness model, (b) the initial slowness model, (c) the model difference between (a) and (b).

where s_i , s_{i+1} is the slowness of i^{th} and $(i+1)^{th}$ layer, respectively; Δ is the difference. For the one-way depth migration, we choose the trace integration algorithm in frequency domain to convert the migration result to model perturbation. The formula for this algorithm can be derived from equation 9. First, we convert the depth-domain reflectivity trace into time domain, next use Fourier transform to transfer the time-domain reflectivity into frequency domain, then taking integration in frequency domain, finally using inverse Fourier transform, we have:

$$s = s_0 \exp\left\{F^{-1}\left\{-2\frac{\widetilde{R}(\omega)}{j\omega}\right\}\right\}, \tag{10}$$

where s_0 is the first slowness in each trace; $\widetilde{R}(\omega)$ is the reflectivity in frequency domain, which comes from PSPI migration of the data residual; j is the imaginary unit; ω is the angular frequency; and $F^{-1}\{\cdot\}$ is the inverse Fourier transform. To ensure that the inversion result s represents the model perturbation, the mean value must be subtracted, and the perturbation needs to be converted into depth domain. For the two-way depth migration, we use equation 8 to directly obtain slowness perturbation:

$$\Delta s = -2sR_i. \tag{11}$$

Why do we choose the inversion algorithm in this way? We use a partial anticline model displayed in figure 1a to answer this question. Figure 1b is the initial model and Figure 1c is the difference between the true model and the initial model. We use many shots and receivers to obtain synthetic data and record seismic data, then perform PSPI migration and RTM with them. Figure 2a displays the PSPI migration result of the data residual (the difference between synthetic data sets of the true model and initial model), and the corresponding impedance inversion using the trace integration in frequency domain is displayed in Figure 1c. Figure 2b displays the RTM result of the data residual, and the corresponding impedance inversion is displayed in Figure 2d. In Figure 2e, the results in Figure 2b and 2d at trace 3km are displayed. From it, we can see that after taking the trace integration algorithm to the PSPI migration result, the phase misfit problem has been fixed greatly, although it cannot be fixed completely or match the phase of real slowness difference as well as RTM. It works because the trace integration algorithm can generate a -90-degree phase shift to the reflectivity trace. Figure 2e also illustrates that there is no obvious phase problem for RTM, so we use equation 11 as the impedance inversion algorithm which do not generate phase change.

The reason why we use the trace integration algorithm in frequency domain rather than in depth or time domain is that there is no accumulated error in the model perturbation

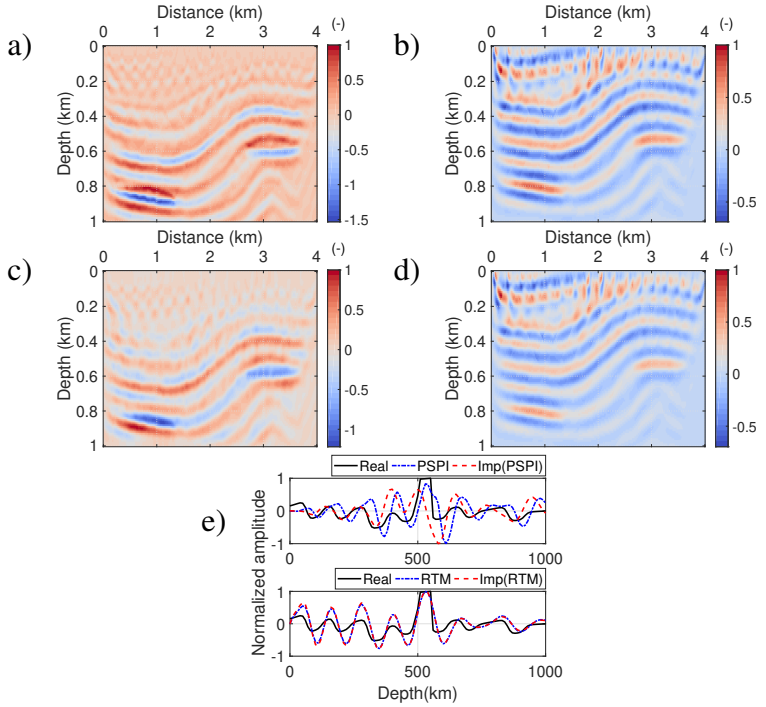

FIG. 2. (a) The result of PSPI migration of the data residual, (b) the result of RTM of the data residual, (c) the result of using impedance inversion to (a), (d) the result of using impedance inversion to (b), and (e) are the results of (c) and (d) at trace 3km.

in frequency domain when compared with that in depth or time domain. It is illustrated in figure 3a-b where we use a 1D model to test the trace integration algorithm in three domains which are sequentially performed with the same noisy data. And all results are converted into depth domain and normalized and removed the mean value. In figure 3b, we can see that the accumulated errors exist in depth and time domains instead of in frequency domain, which will cause underestimation or overestimation of model parameters during the waveform inversion.

Difference between FWI and IMMI

From the workflow of IMMI, we can see that the process is very similar to FWI, the difference is only in the calculation of the model perturbation. For FWI using the steepest descent (SD) method with the preconditioning of deconvolution imaging condition (Margrave et al., 2011a; Pan et al., 2014), the corresponding slowness perturbation further derived from equation 5 and 6 is:

$$\Delta s_{FWI}(\mathbf{x}) = \mu \sum_{r=1}^{ng} \sum_{i=1}^{ns} \int_0^{t_{max}} dt \left[2s(\mathbf{x}) \frac{\ddot{u}_{syn}(\mathbf{x}, t; \mathbf{x}_s) \delta u(\mathbf{x}, t; \mathbf{x}_r)}{u_{syn}(\mathbf{x}, t; \mathbf{x}_s) u_{syn}(\mathbf{x}, t; \mathbf{x}_s) + \lambda I_{max}} \right], \quad (12)$$

where $I_{max} = \max_{\mathbf{x},t} [u_{syn}(\mathbf{x}, t; \mathbf{x}_s) u_{syn}(\mathbf{x}, t; \mathbf{x}_s)]$ is the square of the maximum absolute value in forward propagation wavefield, and λ is the damp factor.

For IMMI using PSPI migration with the deconvolution imaging condition and the

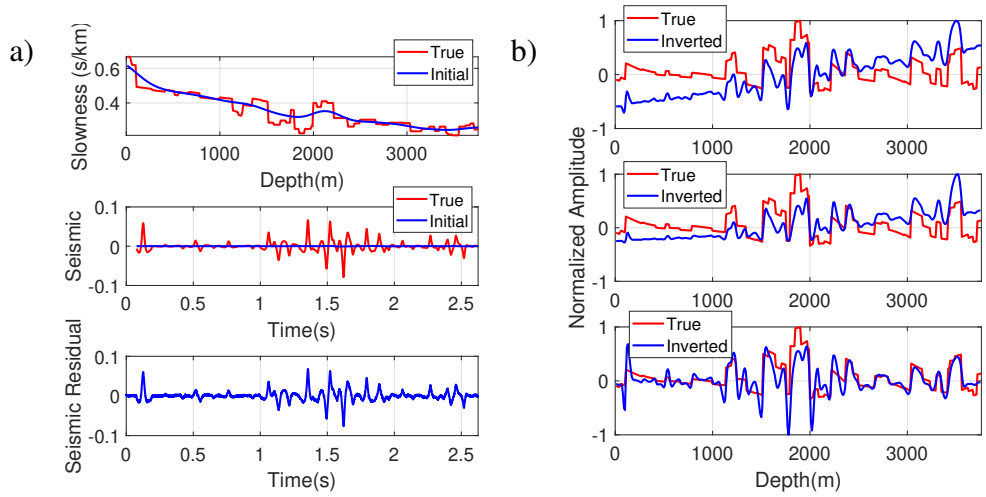

FIG. 3. (a) The 1D model and synthetic seismic data. (b) Trace integration results in depth, time and frequency domain from up to down, respectively.

impedance inversion of equation (9), the slowness perturbation is:

$$\Delta s_{PSPI}(\mathbf{x}) = \mu \mathbf{Imp}\left\{\sum_{r=1}^{ng}\sum_{i=1}^{ns}\int_0^{t_{max}} dt\left[(\mathbf{x})\frac{\ddot{u}_{syn}(\mathbf{x},t;\mathbf{x}_s)\delta u(\mathbf{x},t;\mathbf{x}_r)}{u_{syn}(\mathbf{x},t;\mathbf{x}_s)u_{syn}(\mathbf{x},t;\mathbf{x}_s)+\lambda I_{max}}\right]\right\}, \tag{13}$$

where $\mathbf{Imp}\{\cdot\}$ represents the process of impedance inversion, specifically, it represents the trace integration algorithm in frequency domain here.

For IMMI using RTM with deconvolution imaging condition and impedance inversion of equation 11, the slowness perturbation is :

$$\begin{aligned}\Delta s_{RTM}(\mathbf{x}) &= \mu \mathbf{Imp}\left\{\sum_{r=1}^{ng}\sum_{i=1}^{ns}\int_0^{t_{max}} dt\left[(\mathbf{x})\frac{\ddot{u}_{syn}(\mathbf{x},t;\mathbf{x}_s)\delta u(\mathbf{x},t;\mathbf{x}_r)}{u_{syn}(\mathbf{x},t;\mathbf{x}_s)u_{syn}(\mathbf{x},t;\mathbf{x}_s)+\lambda I_{max}}\right]\right\} \\ &= \mu\sum_{r=1}^{ng}\sum_{i=1}^{ns}\int_0^{t_{max}} dt\left[-2s(\mathbf{x})\frac{u_{syn}(\mathbf{x},t;\mathbf{x}_s)\delta u(\mathbf{x},t;\mathbf{x}_r)}{u_{syn}(\mathbf{x},t;\mathbf{x}_s)u_{syn}(\mathbf{x},t;\mathbf{x}_s)+\lambda I_{max}}\right].\end{aligned} \tag{14}$$

Formula (11) and formula 14 show that the slowness perturbation of FWI is very similar to that of IMMI using RTM. The difference is that the second derivative with respect to time of the forward wave field is required in FWI, but not in IMMI using RTM. However, in IMMI using RTM, there is a negative sign more than FWI, which has the same effect of phase inversion as the second derivative in FWI. Of course, the perturbation values in two equations are unequal. Different from equations 12 and 14 in which the forward and backward wavefields are computed based on the two-way wave equation, in equation 13 the forward and backward wavefields are computed based on the one-way wave equation. Generally, the former is more adaptable, while the later is faster (Mulder and Plessix, 2004).

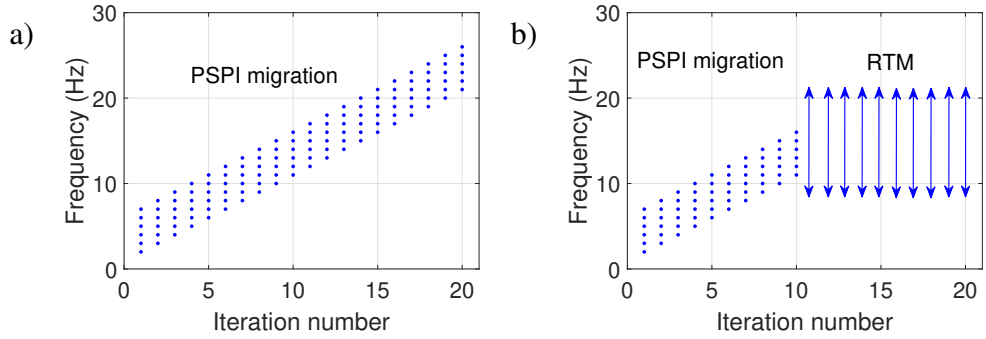

FIG. 4. The inversion strategy in frequency for scheme II (a) and scheme V (b).

Inversion schemes

Scheme I, a standard FWI process with SD method using equation 12 as the model perturbation, noted as FWI. Scheme II, IMMI using PSPI migration and the multiscale inversion strategy, which is also a recommendation from the IMMI workflow (Margrave, 2012) , the model perturbation in given in equation 13, and the multiscale strategy is shown in Figure 4a, this scheme is noted as IMMI PSPImul. As a comparison of scheme II, scheme III is the same as scheme II but no use of the multiscale strategy, which means using all frequencies simultaneously, noted as IMMI PSPIall. Scheme IV is IMMI using RTM which is of the model perturbation equation 14, noted as IMMI RTM. Scheme V, we develop a combined IMMI method, in the first-half iterations (ten iterations are the half for this paper), we use scheme II which uses the multiscale inversion strategy, after that, we use scheme IV until the end of the inversion, the inversion strategy in frequency is shown in figure 4b. Scheme V is noted as IMMI PSPI+RTM.

Numerical examples

In this section, we use two models to test and compare the five waveform inversion schemes. The first one is a partial anticline in figure 5a, which is shown in velocity (km/s), the same model in figure 1a shown in slowness (s/km). The initial model shown in figure1b in slowness (s/km) is the real model after gauss filtering with the window width 200m. This model contains 121*451 grid cells with the grid interval 10 m. The shot number is 19 starting from distance 240m to 4440m with a 240m interval at the top of the model, and the source is a minimum phase Ricker wavelet which 10 Hz dominant frequency. The 451 receivers are also separately set on the top at each grid point.

The inverted models after 20 iterations using the five different inversion schemes are shown in Figure 5b-f. From the inversions, we can see that except scheme III (IMMI PSPIall), all the other schemes can obtain relatively good results. In Figure 5b, the result inverted by scheme I (FWI) suffers from heavy shot footprints, which makes a low quality of near-surface inversion. The result in Figure 5c from scheme II (IMMI PSPImul) occurs stratigraphic incoherence. The result from scheme III (IMMI RTM) has slighter shot footprints when compared with scheme I and better coherence when compared with scheme II. Generally, the result in Figure 5f inverted by scheme V (IMMI PSPI+RTM) provides the best result, which is of little shot footprints and good coherence. In Figure 6a-e, to compare

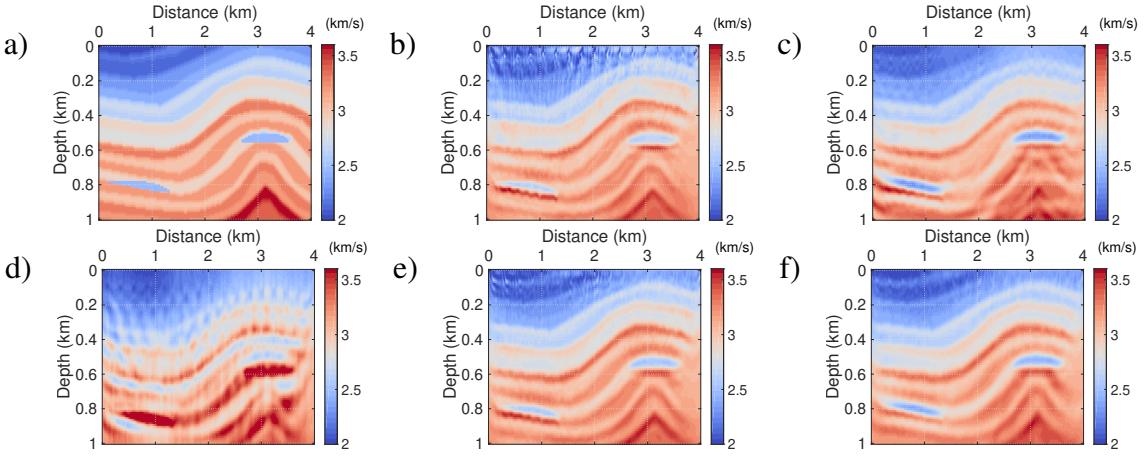

FIG. 5. (a)The true model, (b)-(f) are inverted results of scheme I, II, III, IV and V, respectively.

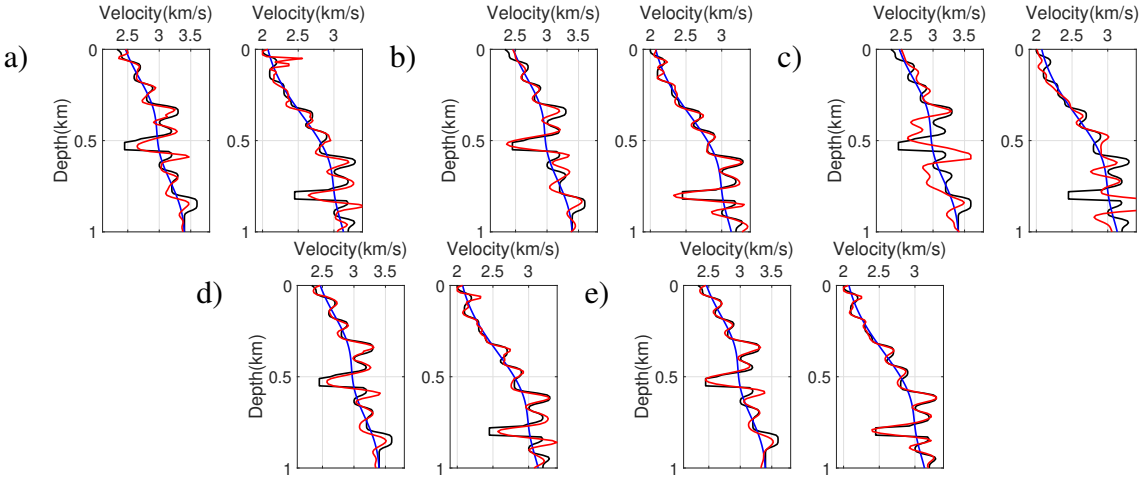

FIG. 6. (a)-(e) are inverted results of scheme I, II, III, IV and V , respectively, at location 860m and 3160m. The black curves are true models, the blue curves are initial models, and the red curves are inverted results.

the results more intuitively, we randomly show results of two traces at distance 860m and 3160m. The comparison also tells us that the result from IMMI PSPI+RTM is the best. In Figure 7a-b, we show the curves of data misfit versus iteration number and mode error versus iteration number. We can see that IMMI PSPIall does not work well, after 20 iterations, FWI has lower data misfit but higher model error than IMMI PSPImul, and IMMI RTM is better than FWI and IMMI PSPImul. Totally, IMMI PSPI+RTM can generate the lowest data misfit and model error.

The inverted results are shown in Figure 8c-g, the overall situation is slightly different from that in the first model. In this case, IMMI PSPIall still does not work well, shot footprints exist both in FWI seriously and in IMMI RTM less seriously. And it seems that 20 iterations are not enough for FWI and IMMI RTM to converge to satisfactory results, but it allows IMMI PSPImul to obtain a relatively good inversion. Although the result from IMMI PSPImul is better than that from FWI and IMMI RTM, it is a crude model in which the edges of faults cannot be depicted clearly. The best result is still from IMMI PSPI+RTM, in which the edges of faults are clearer than that from IMMI PSPImul, and

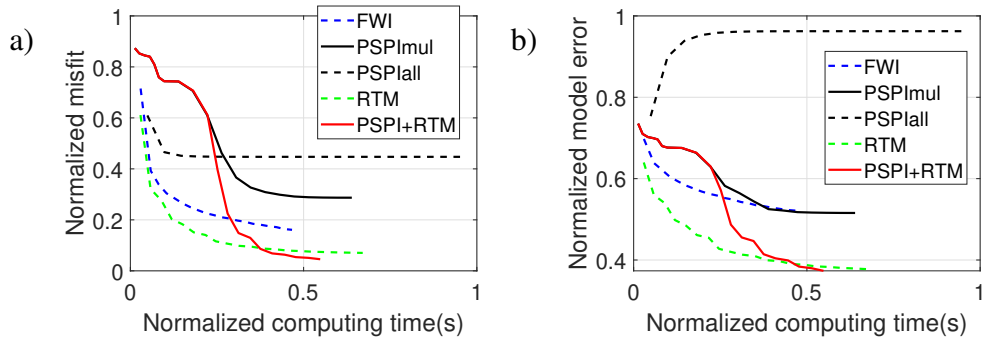

FIG. 7. (a) Data misfit and (b) model error versus iteration number.

the model convergence degree is higher than that from FWI and IMMI RTM. The inverted results at location 860m and 3160m are shown in Figure 9a-e , which gives the same conclusions above.

In figure 10a-b, we show the curves of data misfit and model error versus computing time. Different from the first example, IMMI PSPImul has a better convergence than FWI and IMMI RTM in model error, however, its data misfit is worse than them. In the first several iterations, model error of IMMI PSPImul reduces sharply, but after that data misfit and model error are almost unchanged and stay on a relatively high level. The reason may be that PSPI migration forces on primary waves which can help to reconstruct a crude model quickly, but the data misfit caused by other waves, such as multiples, cannot be fixed. IMMI PSPI+RTM uses RTM as a modifier. First it uses IMMI PSPImul to establish a crude model rapidly, then uses IMMI RTM to construct more details. We can also see that IMMI PSPImul can obtain the crude model in a short time, and IMMI PSPI+RTM is faster than others and gives the lowest model error.

CONCLUSIONS

To examine the IMMI waveform inversion method in the absence of well log data, we perform IMMI using the one-way and two-way wave-equation migration separately and investigate how to select impedance inversion algorithms for different migration algorithms. We suggest that the trace integration algorithm in frequency domain for one-way wave-equation migration, the impedance inversion algorithm without phase change for two-way wave-equation migration.

We have developed a combined IMMI method which uses the one-way depth migration (PSPI migration) and the two-way depth migration (RTM) sequentially in IMMI. The comparisons of inverted results from the five schemes show that the combined method is the fastest and can provides the best inverted model. Also, we can see that either FWI or IMMI using RTM cannot obtain a good near surface inversion, specially, the FWI method. And IMMI using RTM is better than FWI. Furthermore, IMMI using PSPI migration can lower the model error faster than FWI and IMMI using RTM in the complicate model case, but it fails to give clear edges of faults and only works for the multiscale strategy.

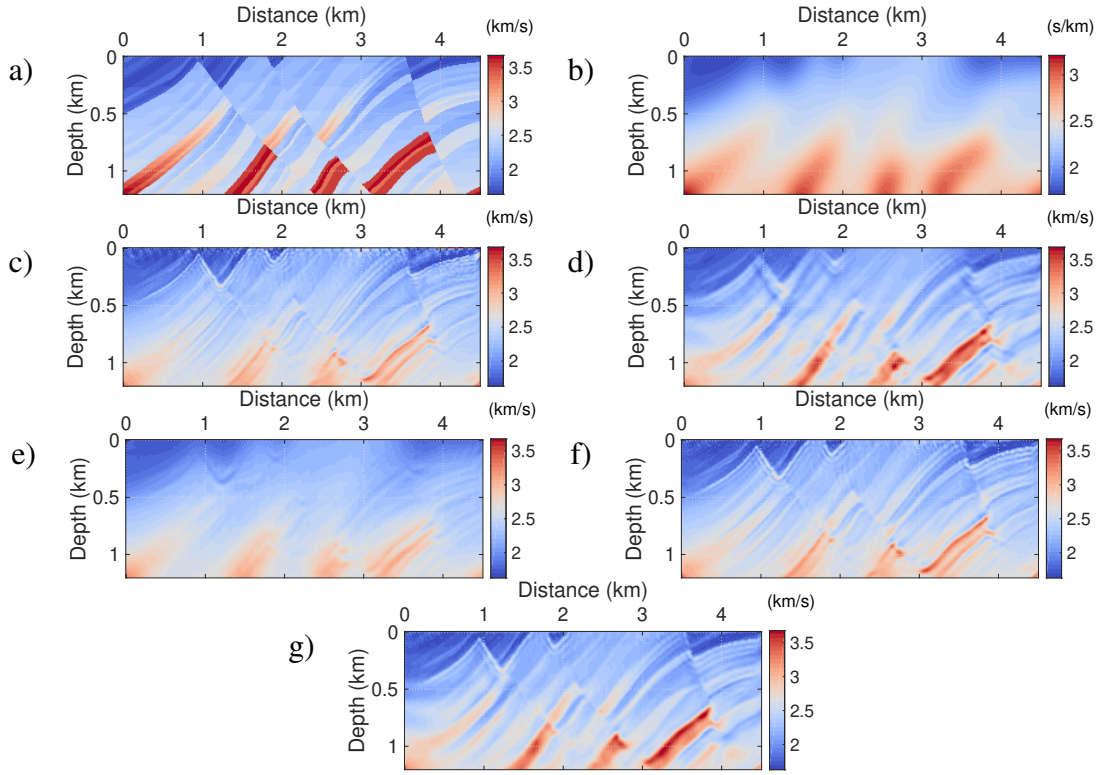

FIG. 8. (a)The true model, (b) the initial model, (c)-(g) are inverted results of scheme I, II, III, IV and V, respectively.

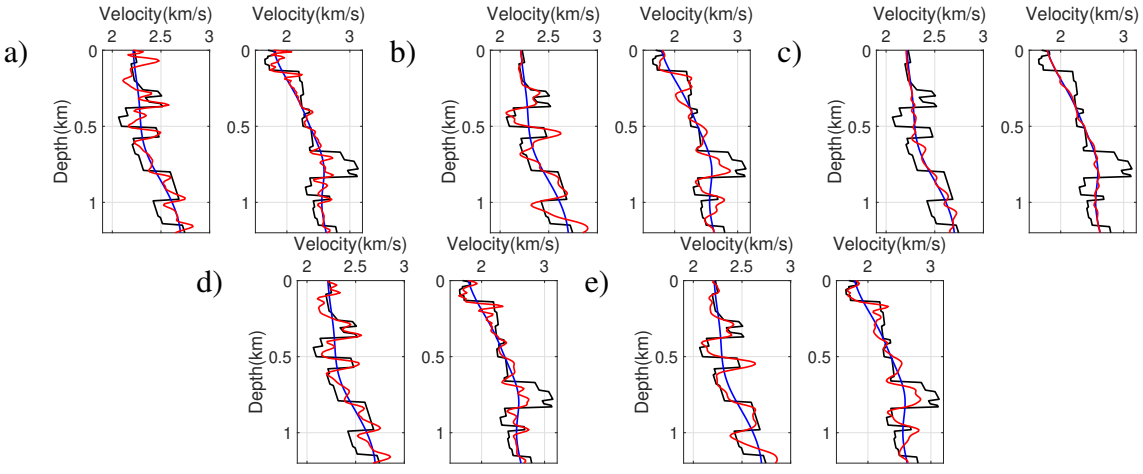

FIG. 9. (a)-(e) are inverted results of scheme I, II, III, IV and V, respectively, at location 860m and 3160m. The black curves are true models, the blue curves are initial models, and the red curves are inverted results.

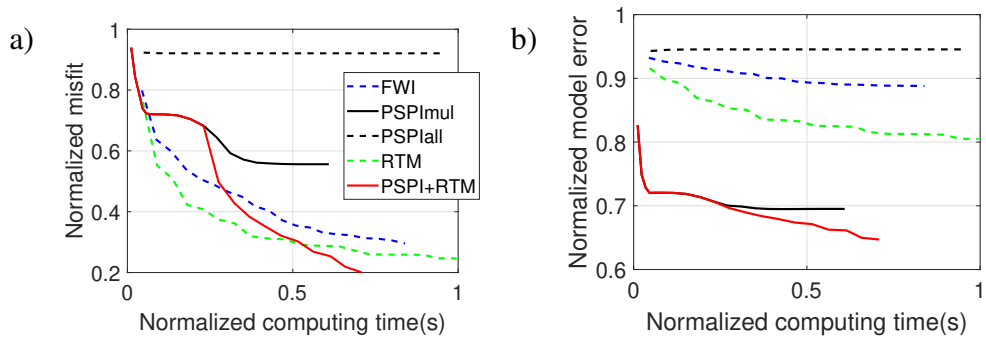

FIG. 10. (a) data misfit and (b) model error versus computing time.

ACKNOWLEDGEMENTS

We thank the sponsors of CREWES for continued support. This work was funded by CREWES industrial sponsors, and NSERC (Natural Science and Engineering Research Council of Canada) through the grant CRDPJ 461179-13.

REFERENCES

Crase, E., Pica, A., Noble, M., McDonald, J., and Tarantola, A., 1990, Robust elastic nonlinear waveform inversion: Application to real data: Geophysics, **55**, No. 5, 527–538.

Gazdag, J., and Sguazzero, P., 1984, Migration of seismic data by phase shift plus interpolation: Geophysics, **49**, No. 2, 124–131.

Guarido, M., Lines, L., and Ferguson, R., 2015, Full waveform inversion: a synthetic test using pspi migration, *in* SEG Technical Program Expanded Abstracts 2015, Society of Exploration Geophysicists, 1456–1460.

Hu, W., Abubakar, A., Habashy, T., and Liu, J., 2011, Preconditioned non-linear conjugate gradient method for frequency domain full-waveform seismic inversion: Geophysical Prospecting, **59**, No. 3, 477–491.

Lailly, P., and Bednar, J., 1983, The seismic inverse problem as a sequence of before stack migrations, *in* Conference on inverse scattering: theory and application, Siam Philadelphia, PA, 206–220.

Margrave, G., Yedlin, M., and Innanen, K., 2011a, Full waveform inversion and the inverse hessian: the 23rd Annual Research Report of the CREWES Project.

Margrave, G. F., 2015, Post-stack iterative modeling migration and inversion (immi), Tech. rep., CREWES Research Report 27: 1–17.

Margrave, G. F., Ferguson, R., and Hogan, C. M., 2010, Full waveform inversion with wave equation migration and well control: the 22nd Annual Research Report of the CREWES Project.

Margrave, G. F., Ferguson, R. J., and Hogan, C. M., 2011b, Full waveform inversion using wave-equation depth migration with tying to wells, *in* SEG Technical Program Expanded Abstracts 2011, Society of Exploration Geophysicists, 2454–2458.

Margrave, G. F., Innanen, K., and Yedlin, M., 2012, A perspective on full waveform inversion: CREWES Res. Rep., **24**, 1–18.

Mora, P., 1987, Nonlinear two-dimensional elastic inversion of multioffset seismic data: Geophysics, **52**, No. 9, 1211–1228.

Mulder, W. A., and Plessix, R.-E., 2004, A comparison between one-way and two-way wave-equation migration: Geophysics, **69**, No. 6, 1491–1504.

Pan, W., Margrave, G. F., and Innanen, K. A., 2014, Iterative modeling migration and inversion (immi): Combining full waveform inversion with standard inversion methodology, *in* SEG Technical Program Expanded Abstracts 2014, Society of Exploration Geophysicists, 938–943.

Romahn, S., and Innanen, K. A., 2017, Iterative modeling, migration, and inversion: Evaluating the well-calibration technique to scale the gradient in the full-waveform inversion process, *in* SEG Technical Program Expanded Abstracts 2017, Society of Exploration Geophysicists, 1583–1587.

Romahn, S. J., and Innanen, K., 2018, Fwi with wave equation migration: well validation vs data validation vs well-and-data validation: CREWES Res. Rep., **30**, 1–12.

Shin, C., Jang, S., and Min, D.-J., 2001, Improved amplitude preservation for prestack depth migration by inverse scattering theory: Geophysical prospecting, **49**, No. 5, 592–606.

Tarantola, A., 1984, Inversion of seismic reflection data in the acoustic approximation: Geophysics, **49**, No. 8, 1259–1266.

Vigh, D., Starr, E. W., and Kapoor, J., 2009, Developing earth models with full waveform inversion: The Leading Edge, **28**, No. 4, 432–435.

Virieux, J., and Operto, S., 2009, An overview of full-waveform inversion in exploration geophysics: Geophysics, **74**, No. 6, WCC1–WCC26.

Yang, P., Gao, J., and Wang, B., 2015, A graphics processing unit implementation of time-domain full-waveform inversion: Geophysics, **80**, No. 3, F31–F39.